AGU PUBLICATIONS

Geophysical Research Letters

RESEARCH LETTER
10.1002/2017GL076751

Key Points:
- Pore-scale modeling reveals that Archie's porosity exponent in dilute granular materials is exclusively related to particle properties
- For nondilute granular materials, the exponent *m* increases continuously as the porosity decreases
- Numerical results suggest a unique correlation between pore throat volume and normalized *m* in nondilute granular materials

Supporting Information:
- Supporting Information S1

Correspondence to:
C. Zhang,
chizhang@ku.edu

Citation:
Niu, Q., & Zhang, C. (2018). Physical explanation of Archie's porosity exponent in granular materials: A process-based, pore-scale numerical study. *Geophysical Research Letters*, *45*, 1870–1877. https://doi.org/10.1002/2017GL076751

Received 17 DEC 2017
Accepted 7 FEB 2018
Accepted article online 12 FEB 2018
Published online 20 FEB 2018

Physical Explanation of Archie's Porosity Exponent in Granular Materials: A Process-Based, Pore-Scale Numerical Study

Qifei Niu[1] and **Chi Zhang**[1]

[1]Department of Geology, The University of Kansas, Lawrence, KS, USA

Abstract The empirical Archie's law has been widely used in geosciences and engineering to explain the measured electrical resistivity of many geological materials, but its physical basis has not been fully understood yet. In this study, we use a pore-scale numerical approach combining discrete element-finite difference methods to study Archie's porosity exponent *m* of granular materials over a wide porosity range. Numerical results reveal that at dilute states (e.g., porosity $\phi >$ ~65%), *m* is exclusively related to the particle shape and orientation. As the porosity decreases, the electric flow in pore space concentrates progressively near particle contacts and *m* increases continuously in response to the intensified nonuniformity of the local electrical field. It is also found that the increase in *m* is universally correlated with the volume fraction of pore throats for all the samples regardless of their particle shapes, particle size range, and porosities.

Plain Language Summary In many topical areas in Earth science and engineering such as groundwater hydrology and petroleum explorations, the electrical resistivity data are widely used to estimate the porosity and/or water/oil content in the subsurface with an empirical relationship that originated in the 1940s of the last century. This relation, known as Archie's law, relates a material's resistivity at saturation to its porosity and the pore fluid resistivity with a power function. As an empirical parameter, the exponent of the function varies considerably among different geological materials, and therefore, the estimated porosity/fluid content is significantly affected by the chosen value. At present, a physical understanding of the exponent is still limited mainly due to the lack of the detailed information on the complex geometry of the pore space. Here we use computational simulations to obtain the microscale geometrical characteristics of synthetic granular materials and to analyze the dominant parameter(s) impacting the exponent. We also provide a pore-scale, mechanistic explanation for the changes in the exponent of granular materials subjected to geological compaction. The findings from this study would help develop a physics-based approach to determine the value of the exponent in the modeling of the resistivity of various Earth materials in practice.

1. Introduction

Electrical and electromagnetic methods play an essential role in imaging and monitoring various properties and processes in both deep and shallow subsurface of the Earth (e.g., Key et al., 2013; St. Clair et al., 2015). To link the measured resistivity to other properties of interest, considerable efforts have been made to develop constitutive models for geological materials (e.g., Bussian, 1983; Ghanbarian et al., 2014; Glover et al, 2000; Sen et al., 1981). The most widely used model is probably Archie's law (Archie, 1942), which relates the conductivity σ of rock to the porosity ϕ by

$$\sigma = \frac{\sigma_w}{F} = \sigma_w \phi^m \tag{1}$$

where σ_w is the pore fluid conductivity, *F* (i.e., ratio of σ_w to σ) is the formation factor, and *m* is the porosity exponent. Archie (1942) found that typical value of *m* is between 1.8 and 2 for sandstones and ~1.3 for unconsolidated sand; however, there are many observations of *m* deviating from the above values (e.g., Friedman, 2005). Equation (1) assumes that rock grains are insulators, and it only considers the current flowing through the bulk solution. For geomaterials with charged surface, the contribution of surface conduction (Revil & Glover, 1998) needs to be excluded from σ to calculate the "intrinsic" value of *F* (Waxman & Smits, 1968).

The physical basis for Archie's law has been the subject of many studies (Hunt, 2004; Mendelson & Cohen, 1982; Sen et al., 1981; Sheng, 1990; Wong et al., 1984), and one key scientific challenge is to reveal the dominant textural control on *m* (Glover, 2009). Theoretical studies (e.g., Mendelson & Cohen, 1982; Sen et al., 1981)

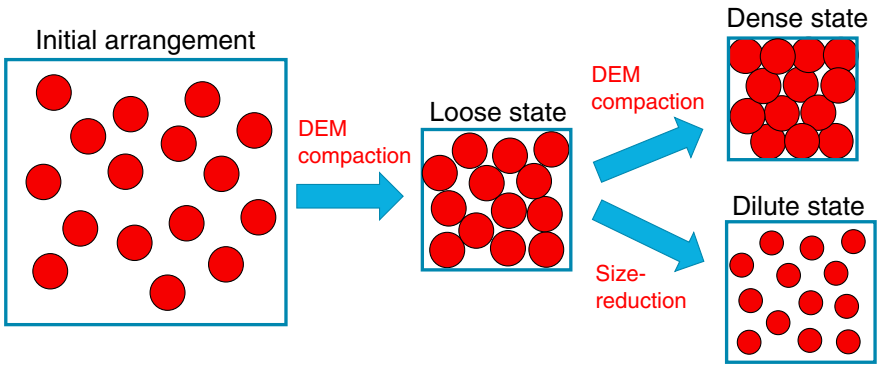

Figure 1. Schematic diagram illustrating the procedure to prepare various states of the samples.

have confirmed the strong dependence of particle properties on *m* as observed in experiments (e.g., Jackson et al., 1978). In addition, numerical and experimental studies have shown profound influences of pore attributes on *m*, including porosity (Borai, 1987; Olsen et al., 2008), tortuosity (Salem & Chilingarian, 1999), the skewness of the pore size distribution (Wong et al., 1984), and connectivity (Bernabé et al., 2011). Moreover, it has also been suggested that *m* might be related to some geological processes such as cementation (Archie, 1942; Leroy et al., 2017; Schwartz & Kimminau, 1987; Wu et al., 2010), compaction (Fatt, 1957; Glover et al., 2000), and mineral dissolution (Garing et al., 2014; Sen et al., 1997). Indeed, the above mentioned factors are not independent but are essentially interrelated in affecting *m*. At present, there is no consensus on the physical meaning of *m* in geological materials and further studies are still necessary to reconcile the existing findings.

In this study, we investigate the controls on *m* in granular materials using a pore-scale numerical approach that combines discrete element-finite difference methods. The samples presented here consist of spherical and oblate particles, and the solid-phase concentration varies broadly, from dilute (i.e., a limited particle-particle interaction; $\phi >$ ~65%) to dense states (i.e., $\phi =$ ~30%). Our work is unique in applying a physics-based approach, that is, discrete element method (Cundall & Strack, 1979), to simulate the compaction of loosely packed granular samples. The effective conductivity of the granular sample is calculated by directly solving the finite difference representation of the Laplace equation (Garboczi, 1998). Furthermore, we use a modified maximal ball algorithm (Dong & Blunt, 2009) to determine the pore attributes of the samples such that the possible link between material's texture and *m* can be revealed.

2. Samples and Methods

2.1. Sample Preparations

Six granular samples are used in the 3-D numerical simulation, and they are assemblies of 8,000 spherical or oblate particles. In each sample, all the particles have the same shape ($e = 1$, 0.67, or 0.5 where e is the ratio of the semiminor to semimajor axes), and the particle size follows either a Dirac delta distribution centered at d or a uniform distribution in the range $[0.5d, 1.5d]$. For all the samples, we use the same procedure to attain a number of states as shown in Figure 1. We start with an initially sparse arrangement, in which the particle locations and orientations are random. The loose state of the sample (e.g., $\phi =$ ~42%) is then obtained by isotropically reducing the boundary dimensions until the sample develops a loading-bearing fabric (e.g., see Kuhn et al., 2014; Sun et al., 2013). Afterward, the dense state of the sample ($\phi =$ ~30%) is attained by further compressing the loose granular assembly. The discrete element method code OVAL developed by Kuhn (2006) (available at http://faculty.up.edu/kuhn/oval/oval.html) is used to model this process, and the details of the simulation are further explained in the supporting information. In addition, we also attain the dilute states (e.g., $\phi >$ ~65%) of the samples by simultaneously reducing the size of all the particles but fixing their locations and orientations at loose states (Figure 1).

2.2. Effective Conductivity Calculation

To calculate the effective electrical conductivity of a sample, a cubic representative elementary volume (REV) is taken out from the granular assembly. The REV is then discretized into a number of voxels with the same

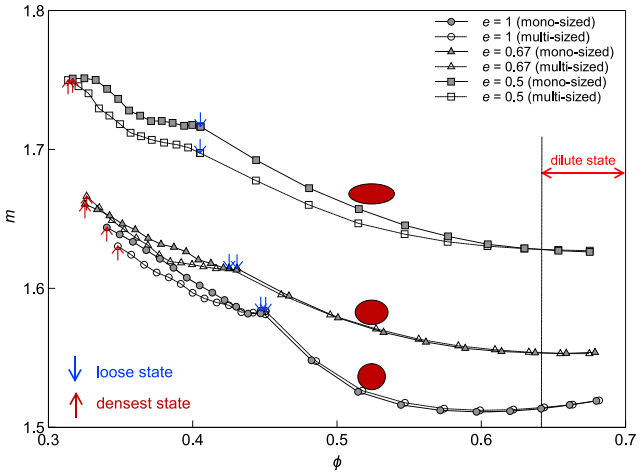

Figure 2. The variation of Archie's porosity exponent m of six granular samples from dilute to dense states.

dimension, and each voxel has a constant conductivity. Subjected to a uniform external electrical field, the spatial current density in the REV can be calculated by solving the finite-difference representation of Laplace equation. In the calculation, the grain conductivity is set to zero to comply with the assumption of equation (1). Based on the volume-averaged current density and electrical field, the effective conductivity of the sample can then be determined by Ohm's law. In this study, we adopted an open source code (DC3D.F) developed at the National Institute of Standards and Technology (available online at http://ciks.cbt.nist.gov/garbocz/manual/node52.html) to realize the numerical calculation (e.g., Andrä et al., 2013; Garboczi, 1998; Niu et al., 2017; Niu & Zhang, 2017; Zhan et al., 2010).

3. Results

The effective electrical conductivity σ of the six saturated granular samples is calculated at 22 states ranging from dilute to dense. In the calculation, the REV has a dimension of 3 mm × 3 mm × 3 mm, and it is discretized into 300^3 voxels. The related m of the samples is determined as $m = -\log_{\phi}(\sigma_w/\sigma)$, and the results are presented in Figure 2. It appears that the exponent m of a granular material is not a constant but a function of ϕ. At dilute state, m roughly keeps constant; as ϕ decreases, m increases continuously. In addition, it is apparent that both particle shape and size range have strong effects on m at a given porosity. In the following, these features will be discussed in detail.

3.1. Effect of Particle Shape

The effect of particle properties on m has been well studied with the differential effective medium theory (Sheng, 1990), which implements a homogenization process that incrementally adds dilute particles to the liquid phase toward a given solid-phase concentration. For granular materials consisting of spheroids, Mendelson and Cohen (1982) have developed an analytical equation linking m to the particle shape and orientation. If the spheroids are randomly orientated, m can be written as (Mendelson & Cohen, 1982; Sen, 1984)

$$m = \frac{5 - 3L}{3(1 - L^2)} \tag{2}$$

where L is the depolarization factor along the semiminor axis, which is directly related to the particle shape (see supporting information). For particles aligned along an electric field with direction i, the related m_i is expressed as (Sen et al., 1981)

$$m_i = \frac{1}{1 - L_i} \tag{3}$$

where L_i is the depolarization factor along direction i. Note that the differential effective medium theory iteratively applies the dilute assumption, and therefore, in principle, equation (2) should only be valid for granular samples at dilute states.

Equations (2) and (3) are used to show the influence of particle shape on m as plotted in Figure 3. Note that equation (3) is for aligned particles, and therefore, the results in directions parallel (||) and perpendicular (⊥) to the semi-major axis can be regarded as two limiting cases of m. For comparison, the porosity exponent of the three monosized samples in Figure 2 at dilute states m_0 is also plotted in the figure. In addition, we include the results of other 29 synthesized dilute granular samples. These samples consist of randomly packed, monosized, oblate particles with e ranging between 0.3 and 1, and they are also prepared with the procedure in Figure 1. As shown in Figure 3, m_0 from

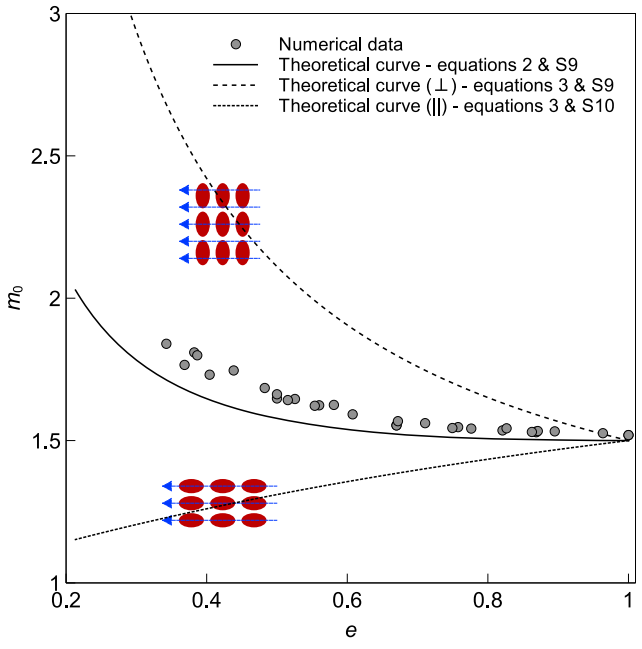

Figure 3. Influences of particle shape and orientation on Archie's porosity exponent of granular materials at dilute states m_0.

numerical simulation and equation (2) shows a similar trend as e varies. In addition, m_0 from simulations is within the upper and lower boundaries described by equation (3). Both numerical and theoretical results indicate that the particle shape controls m_0. For granular materials with randomly oriented particles, as the particle becomes more aspherical, the related m_0 is larger. In general, numerically determined m_0 is slightly higher than theoretical values as shown in Figure 3. This minor discrepancy is due to the use of discrete voxels to represent continuum objects (Arns et al., 2002) in calculating σ (see more discussions in the supporting information).

3.2. Effect of Particle Size Range

Previous studies on the effect of particle size range on m are controversial. For instance, the effective medium theory suggests that m is independent of particle size range (Mendelson & Cohen, 1982; Sen et al., 1981). However, some experimental results have indicated that the particle size range can affect m (e.g., Lemaitre et al., 1988). We believe that the contrasting outcomes are due to different sample states considered. As noted, the differential effective medium theory iteratively applies the dilute assumption; therefore, in principle, their prediction is only applicable for dilute samples. In contrast, Lemaitre et al.'s (1988) experiments were using granular packings, and hence, the observed influence of particle size range on m should only be associated with nondilute samples.

The numerical results in Figure 2 are used to test our above hypothesis. At dilute state, we found that m of multisized and monosized samples with same particle shape is almost identical, suggesting limited effects of particle size range on m. This finding agrees with the differential effective medium theory. As the particles become more concentrated (i.e., porosity decreases), multisized and monosized samples start to have varying m values despite the same particle shape. It appears that samples with a broader particle size range (empty symbols in Figure 2) tend to have a lower m. This observed dependence of particle size range on m of nondilute granular samples is consistent with some experimental data, for example, as reviewed by Friedman (2005).

3.3. Evolution of *m*

In Figure 2, it is shown that the exponent m of granular materials increases with the solid-phase concentration but its physical causes have not been explained. Here we examine the m variation from a pore-scale perspective. Consider a cubic porous medium with length l subjected to an electric potential gradient. The formation factor F is defined as (Johnson et al., 1986)

$$F = \frac{l|\psi|^2}{\int|\mathbf{e}(\mathbf{r})|^2 \mathrm{d}V} \tag{4}$$

where ψ is the potential drop across the sample and $\mathbf{e}(\mathbf{r})$ is the resulting electrical field in the pore space V. Considering equation (1), the microscopic definition of m can be expressed as

$$m = \frac{\ln\left(\int|\mathbf{E}(\mathbf{r})|^2 \mathrm{d}f\right)}{\ln(\int \mathrm{d}f)} \tag{5}$$

where $\mathbf{E}(\mathbf{r})$ is the local electric field $\mathbf{e}(\mathbf{r})$ normalized by ψ/l and df indicates that the integration is over the pore space from 0 to ϕ. According to equation (5), if the local electrical field in the pore space is uniform (e.g., in straight capillary tubes), m is unity because $|\mathbf{E}(\mathbf{r})| = 1$. For porous media with complex pore space, the electrical field is not uniform, which makes m deviate from 1. From this perspective, a change in m of a porous medium is therefore an indication of the spatial variations in $|\mathbf{E}|^2$ in its pore space.

Take the monosized sample with $e = 0.67$ as an example. The electric field in its pore space is calculated at five different states: A, B, C, D, and E. As shown in Figure 4a, A represents the dilute state ($\phi = 67\%$), C corresponds to the loose state ($\phi = 43\%$), E is the densest state ($\phi = 32\%$) after compaction, and B ($\phi = 50\%$) and D ($\phi = 39\%$) are two intermediate states. In Figure 4a, the histograms of $|\mathbf{E}|^2$ at all voxels in the pore space are plotted. It is shown that as the solid-phase concentration increases, the $|\mathbf{E}|^2$ distribution becomes more heterogeneous (or dispersed) and more pore space acquires a high $|\mathbf{E}|^2$ value. For instance, at state A, only a few voxels have a $|\mathbf{E}|^2$ value higher than 100 but at state E, the number increases to $\sim 2 \times 10^4$. The intensified nonuniformity of $|\mathbf{E}|^2$ distribution, according to equation (5), makes m continuously increase as the sample changes from states A to E as shown in Figure 2.

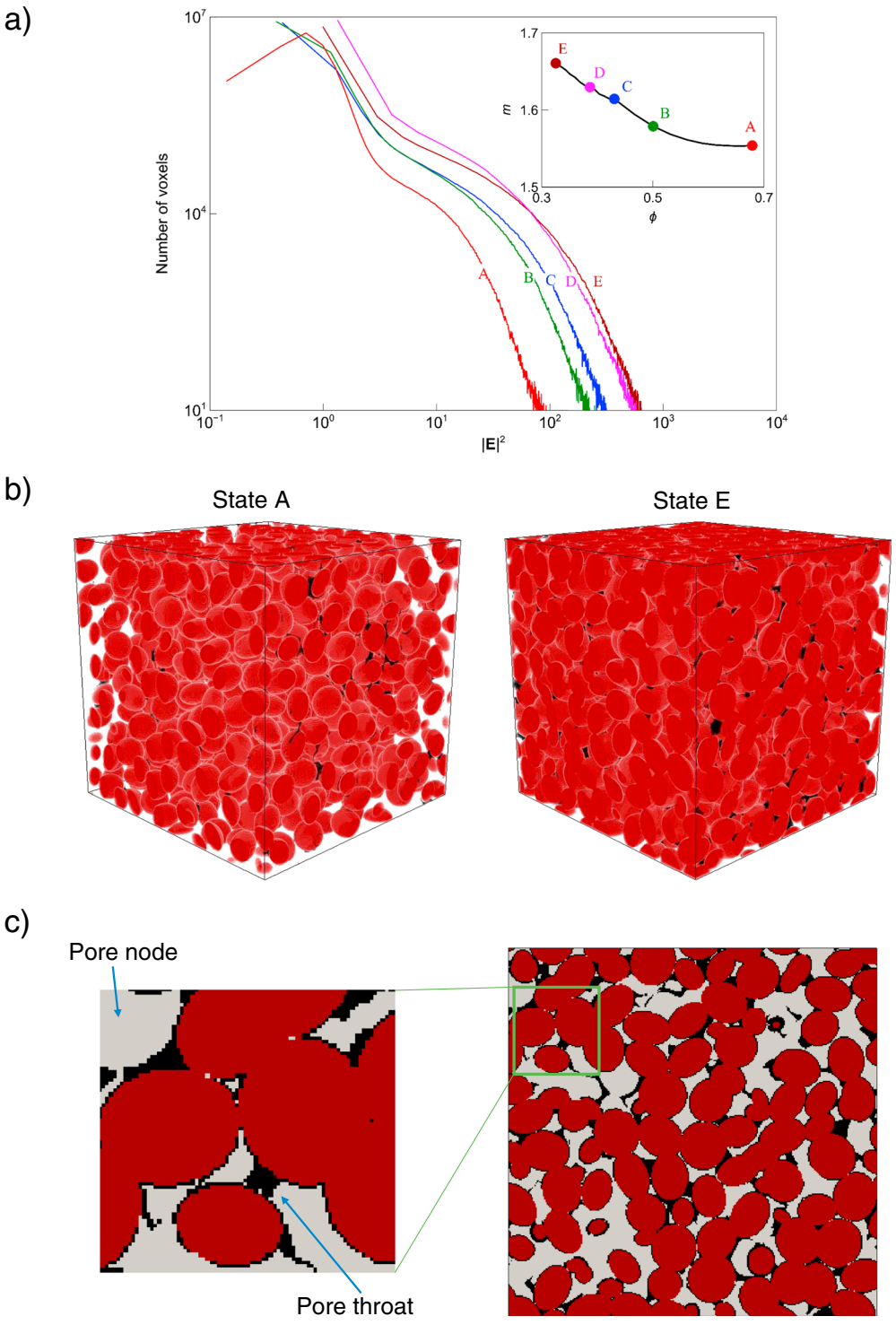

Figure 4. Pore-scale characteristics of the monosized sample with $e = 0.67$: (a) the number of voxels with a given $|\mathbf{E}|^2$ value at five states: A ($\phi = 67\%$), B ($\phi = 50\%$), C ($\phi = 43\%$), D ($\phi = 39\%$), and E ($\phi = 32\%$); (b) 3-D illustration of the microstructure and electric field at states A and E; and (c) 2-D illustration of the microstructure and electric field at state E.

To visualize, we plot the 3-D microstructure and spatial $|\mathbf{E}|^2$ distribution of the sample at states A and E in Figure 4b. In the images, solid particles are highlighted in red and pore space with $|\mathbf{E}|^2 > 50$ is featured in black. Comparing to state A, it is apparent that the sample at state E has a much larger portion of pore space with high $|\mathbf{E}|^2$, indicating intensified nonuniformity of the electrical field strength. Interestingly, we found that

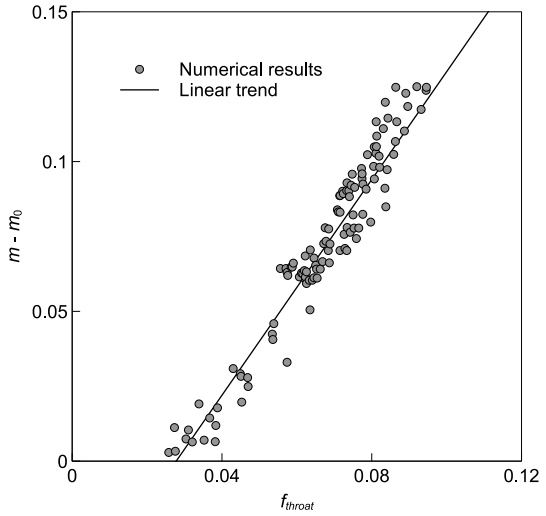

Figure 5. Correlation between the normalized Archie's porosity exponent m-m_0 and the volume fraction of pore throats f_{throat} for all the samples considered in this study.

most of the pores in black are within the region where two particles contact (i.e., the narrow pore throats as shown in Figure 4c). Since a large $|\mathbf{E}|$ is equivalent to a high electric flux density, Figure 4 elucidates that when the granular material moves from the dilute state to a dense state, the electrical flow becomes more concentrated in the pore throats.

4. Discussion

As discussed in section 3.3, the increase of m in granular materials is related to the intensified nonuniformity of the electric field strength $|\mathbf{E}|$ in the pore space and the concentrated electric flow at pore throats. This intrigues us to investigate if m and pore throat volume are correlated. We used a modified maximal ball algorithm (Dong & Blunt, 2009) to determine the pore throat volume for the granular samples. This algorithm applies a clustering process (Dong & Blunt, 2009) to organize the maximal balls into pore throat chains such that the profile of the pore space can be described. According to these chains, the pore space can be segmented into pore node and throats (e.g., see, Blunt et al., 2013).

The results are shown in Figure 5 where the volume fraction of pore throats f_{throat} and normalized porosity exponent m-m_0 are plotted for all the six samples at different states. We suggest to normalize m by subtracting the value at the dilute state m_0 such that individual effect of particles can be isolated from the impact of pore attributes. This treatment may also permit a unified explanation that reconciles that different interpretations of m already existed in the literature. As shown in Figure 5, all the samples collapse into a single linear line regardless of their particle shapes, size ranges, and porosities. This unique trend suggests that there might be a universal correlation between the increase in m (relative to the dilute state of individual samples) and the relative volume of pore throats for granular materials. Further studies are suggested to experimentally verify this correlation.

The positive relation observed in granular materials (Figure 5) can explain many experimental observations regarding m in consolidated sediments. For example, Wong et al. (1984) observed that fused glass beads sample with a broader pore size distribution tends to have a higher m value. From the micrographs in Wong et al. (1984), it is clear that the sample with a broad pore size range is also related to increased pore throat volume fraction. Another example is the Fontainebleau sandstone reported by Revil et al., (2014) where m generally becomes larger as the degree of cementation (silica overgrowth) increases (e.g., their Figure 5a). Their microcomputed tomography images clearly show that as the porosity decreases, the pore space becomes more heterogeneous (i.e., the fraction of pore throat volume increases). In this sense, it seems reasonable to extend our findings in granular materials to sedimentary rocks; however, further studies are still needed to quantitatively verify its applicability.

While applying Archie's law to interpret field resistivity data, m is usually chosen empirically with little theoretical justification. A better understanding of the physical significance of m will directly help geophysicists determine the appropriate values for m and F. In hydrocarbon explorations, an accurate m can significantly improve the reserve calculation from well-logging data (e.g., Glover, 2009; Shankar & Riedel, 2011). In hydrogeophysics, a correct F value is the key to characterizing permeability with either the characteristic pore size-based model (Johnson et al., 1986) or the Kozeny-Carman equation incorporating tortuosity (e.g., Slater et al., 2014). In solid Earth studies, the estimation of porosity and fluid budget in subduction zone from resistivity data will also benefit significantly from a physical understanding of m (Naif et al., 2016).

5. Conclusions

Based on the pore-scale, numerical study, we have reached the following conclusions regarding Archie's porosity exponent m of granular materials. At dilute states (e.g., $\phi > 65\%$), m is exclusively related to particle shape and orientation; this relationship can be quantitatively described with the differential effective

medium theory. As the granular materials deviate from the dilute state toward a denser state, m increases with the solid-phase concentration; in this process, the particle size range has a noticeable effect on m, and samples with a wider size range tend to have a lower m at a given porosity. From dilute to dense states, the increase in m of granular materials is related to the pore-scale variations in the electrical field $|\mathbf{E}|$; in general, a high m value corresponds to a more dispersed distribution of $|\mathbf{E}|^2$ in the pore space. Our numerical results also suggest that for granular materials, a universal relation might exist, which links the volume fraction of pore throats to the increase in m (relative to the value at dilute state m_0) regardless of the particle shape, particle size range, and porosities.

Acknowledgments
The discrete element method code OVAL and finite difference code DC3D.F can be obtained online using the URLs listed in the main text. Other data can be obtained from the corresponding author upon request. The authors would like to thank Martin Blunt at the Imperial College London for providing the pore network extraction code.

References

Andrä, H., Combaret, N., Dvorkin, J., Glatt, E., Han, J., Kabel, M., et al. (2013). Digital rock physics benchmarks—Part II: Computing effective properties. *Computers & Geosciences*, *50*, 33–43. https://doi.org/10.1016/j.cageo.2012.09.008

Archie, G. E. (1942). The electrical resistivity log as an aid in determining some reservoir characteristics. *Petroleum Transactions of AIME*, *146*(01), 54–62. https://doi.org/10.2118/942054-G

Arns, C. H., Knackstedt, M. A., Pinczewski, W. V., & Garboczi, E. J. (2002). Computation of linear elastic properties from microtomographic images: Methodology and agreement between theory and experiment. *Geophysics*, *67*(5), 1396–1405. https://doi.org/10.1190/1.1512785

Bernabé, Y., Zamora, M., Li, M., Maineult, A., & Tang, Y. B. (2011). Pore connectivity, permeability, and electrical formation factor: A new model and comparison to experimental data. *Journal of Geophysical Research*, *116*, B11204. https://doi.org/10.1029/2011JB008543

Blunt, M. J., Bijeljic, B., Dong, H., Gharbi, O., Iglauer, S., Mostaghimi, P., et al. (2013). Pore-scale imaging and modelling. *Advances in Water Resources*, *51*, 197–216. https://doi.org/10.1016/j.advwatres.2012.03.003

Borai, A. (1987). A new correlation for the cementation factor in low-porosity carbonates. *SPE Formation Evaluation*, *2*(04), 495–499. https://doi.org/10.2118/14401-PA

Bussian, A. (1983). Electrical conductance in a porous medium. *Geophysics*, *48*(9), 1258–1268. https://doi.org/10.1190/1.1441549

Cundall, P. A., & Strack, O. D. L. (1979). A discrete numerical model for granular assemblies. *Géotechnique*, *29*(1), 47–65. https://doi.org/10.1680/geot.1979.29.1.47

Dong, H., & Blunt, M. J. (2009). Pore-network extraction from micro-computerized-tomography images. *Physical Review E*, *80*(3), 036307. https://doi.org/10.1103/PhysRevE.80.036307

Fatt, I. (1957). Effect of overburden and reservoir pressure on electric logging formation factor. *AAPG Bulletin*, *41*(11), 2456–2466.

Friedman, S. P. (2005). Soil properties influencing apparent electrical conductivity: A review. *Computers and Electronics in Agriculture*, *46*(1-3), 45–70. https://doi.org/10.1016/j.compag.2004.11.001

Garboczi, E. J. (1998). Finite element and finite difference programs for computing the linear electric and elastic properties of digital images of random materials.

Garing, C., Luquot, L., Pezard, P. A., & Gouze, P. (2014). Electrical and flow properties of highly heterogeneous carbonate rocks. *AAPG Bulletin*, *98*(1), 49–66. https://doi.org/10.1306/05221312134

Ghanbarian, B., Hunt, A. G., Ewing, R. P., & Skinner, T. E. (2014). Universal scaling of the formation factor in porous media derived by combining percolation and effective medium theories. *Geophysical Research Letters*, *41*, 3884–3890. https://doi.org/10.1002/2014GL060180

Glover, P. (2009). What is the cementation exponent? A new interpretation. *The Leading Edge*, *28*(1), 82–85. https://doi.org/10.1190/1.3064150

Glover, P. W., Hole, M. J., & Pous, J. (2000). A modified Archie's law for two conducting phases. *Earth and Planetary Science Letters*, *180*(3-4), 369–383. https://doi.org/10.1016/S0012-821X(00)00168-0

Glover, P. W. J., Gómez, J. B., & Meredith, P. G. (2000). Fracturing in saturated rocks undergoing triaxial deformation using complex electrical conductivity measurements: Experimental study. *Earth and Planetary Science Letters*, *183*(1-2), 201–213. https://doi.org/10.1016/S0012-821X(00)00267-3

Hunt, A. G. (2004). Continuum Percolation Theory and Archie's Law. *Geophysical Research Letters*, *31*, L19503. https://doi.org/10.1029/2004GL020817

Jackson, P. D., Smith, D. T., & Stanford, P. N. (1978). Resistivity-porosity-particle shape relationships for marine sands. *Geophysics*, *43*(6), 1250–1268. https://doi.org/10.1190/1.1440891

Johnson, D. L., Koplik, J., & Schwartz, L. M. (1986). New pore-size parameter characterizing transport in porous media. *Physical Review Letters*, *57*(20), 2564–2567. https://doi.org/10.1103/PhysRevLett.57.2564

Key, K., Constable, S., Liu, L., & Pommier, A. (2013). Electrical image of passive mantle upwelling beneath the northern East Pacific rise. *Nature*, *495*(7442), 499–502. https://doi.org/10.1038/nature11932

Kuhn, M. R. (2006). *OVAL and OVALPLOT: Programs for Analyzing Dense Particle Assemblies With the Discrete Element Method*. Retrieved from http://faculty.up.edu/kuhn/oval/doc/oval_0618.pdf

Kuhn, M. R., Renken, H. E., Mixsell, A. D., & Kramer, S. L. (2014). Investigation of cyclic liquefaction with discrete element simulations. *Journal of Geotechnical and Geoenvironmental Engineering*, *140*(12), 04014075. https://doi.org/10.1061/(ASCE)GT.1943-5606.0001181

Lemaitre, J., Troadec, J. P., Bideau, D., Gervois, A., & Bougault, E. (1988). The formation factor of the pore space of binary mixtures of spheres. *Journal of Physics D: Applied Physics*, *21*(11), 1589–1592. https://doi.org/10.1088/0022-3727/21/11/007

Leroy, P., Li, S., Jougnot, D., Revil, A., & Wu, Y. (2017). Modelling the evolution of complex conductivity during calcite precipitation on glass beads. *Geophysical Journal International*, *209*(1), 123–140.

Mendelson, K. S., & Cohen, M. H. (1982). The effect of grain anisotropy on the electrical properties of sedimentary rocks. *Geophysics*, *47*(2), 257–263. https://doi.org/10.1190/1.1441332

Naif, S., Key, K., Constable, S., & Evans, R. L. (2016). Porosity and fluid budget of a water-rich megathrust revealed with electromagnetic data at the Middle America Trench. *Geochemistry, Geophysics, Geosystems*, *17*, 4495–4516. https://doi.org/10.1002/2016GC006556

Niu, Q., Revil, A., Li, Z., & Wang, Y.-H. (2017). Relationship between electrical conductivity anisotropy and fabric anisotropy in granular materials during drained triaxial compressive tests: A numerical approach. *Geophysical Journal International*, *210*(1), 1–17. https://doi.org/10.1093/gji/ggx140

Niu, Q., & Zhang, C. (2017). Pore-scale numerical modeling of complex conductivity of saturated granular materials. *Near Surface Geophysics*, *15*(6), 593–602.

Olsen, C., Hongdul, T., & Fabricius, I. L. (2008). Prediction of Archie's cementation factor from porosity and permeability through specific surface. *Geophysics*, *73*(2), E81–E87. https://doi.org/10.1190/1.2837303

Revil, A., & Glover, P. W. J. (1998). Nature of surface electrical conductivity in natural sands, sandstones, and clays. *Geophysical Research Letters*, *25*(5), 691–694. https://doi.org/10.1029/98GL00296

Revil, A., Kessouri, P., & Torres-Verdín, C. (2014). Electrical conductivity, induced polarization, and permeability of the Fontainebleau sandstone. *Geophysics*, *79*(5), D301–D318. https://doi.org/10.1190/geo2014-0036.1

Salem, H. S., & Chilingarian, G. V. (1999). The cementation factor of Archie's equation for shaly sandstone reservoirs. *Journal of Petroleum Science and Engineering*, *23*(2), 83–93. https://doi.org/10.1016/S0920-4105(99)00009-1

Schwartz, L. M., & Kimminau, S. (1987). Analysis of electrical conduction in the grain consolidation model. *Geophysics*, *52*(10), 1402–1411. https://doi.org/10.1190/1.1442252

Sen, P. N. (1984). Grain shape effects on dielectric and electrical properties of rocks. *Geophysics*, *49*(5), 586–587. https://doi.org/10.1190/1.1441695

Sen, P. N., Kenyon, W. E., Takezaki, H., & Petricola, M. J. (1997). Formation factor of carbonate rocks with microporosity: Model calculations. *Journal of Petroleum Science and Engineering*, *17*(3-4), 345–352. https://doi.org/10.1016/S0920-4105(96)00005-8

Sen, P. N., Scala, C., & Cohen, M. H. (1981). A self-similar model for sedimentary-rocks with application to the dielectric-constant of fused glass-beads. *Geophysics*, *46*(5), 781–795. https://doi.org/10.1190/1.1441215

Shankar, U., & Riedel, M. (2011). Gas hydrate saturation in the Krishna-Godavari basin from P-wave velocity and electrical resistivity logs. *Marine and Petroleum Geology*, *28*(10), 1768–1778. https://doi.org/10.1016/j.marpetgeo.2010.09.008

Sheng, P. (1990). Effective-medium theory of sedimentary rocks. *Physical Review B*, *41*(7), 4507–4512. https://doi.org/10.1103/PhysRevB.41.4507

Slater, L., Barrash, W., Montrey, J., & Binley, A. (2014). Electrical-hydraulic relationships observed for unconsolidated sediments in the presence of a cobble framework. *Water Resources Research*, *50*, 5721–5742. https://doi.org/10.1002/2013WR014631

St. Clair, J., Moon, S., Holbrook, W. S., Perron, J. T., Riebe, C. S., Martel, S. J., et al. (2015). Geophysical imaging reveals topographic stress control of bedrock weathering. *Science*, *350*(6260), 534–538. https://doi.org/10.1126/science.aab2210

Sun, W., Kuhn, M. R., & Rudnicki, J. W. (2013). A multiscale DEM-LBM analysis on permeability evolutions inside a dilatant shear band. *Acta Geotechnica*, *8*(5), 465–480. https://doi.org/10.1007/s11440-013-0210-2

Waxman, M., & Smits, L. (1968). A electrical conductivities in oil-bearing shaly sands. *Old SPE Journal*, *8*(02), 107–122. https://doi.org/10.2118/1863-A

Wong, P.-Z., Koplik, J., & Tomanic, J. (1984). Conductivity and permeability of rocks. *Physical Review B*, *30*(11), 6606–6614. https://doi.org/10.1103/PhysRevB.30.6606

Wu, Y., Hubbard, S., Williams, K. H., & Ajo-Franklin, J. (2010). On the complex conductivity signatures of calcite precipitation. *Journal of Geophysical Research*, *115*, G00G04. https://doi.org/10.1029/2009JG001129

Zhan, X., Schwartz, L. M., Toksöz, M. N., Smith, W. C., & Morgan, F. D. (2010). Pore-scale modeling of electrical and fluid transport in Berea sandstone. *Geophysics*, *75*(5), F135–F142. https://doi.org/10.1190/1.3463704